Dynamics of phosphate head groups in biomembranes

Comprehensive analysis using phosphorus-31 nuclear magnetic resonance lineshape and relaxation time measurements

Erick J. Dufourc*, Christian Mayer‡, Jürgen Stohrer‡, Gerhard Althoff‡, and Gerd Kothe‡

*Centre de Recherche Paul Pascal, CNRS, Av. A. Schweitzer 33600 Pessac France; and ‡Department of Physical Chemistry, University of Stuttgart, Pfaffenwaldring 55, 7000 Stuttgart 80, Germany

ABSTRACT Phospholipid head group dynamics have been studied by pulsed phosphorus-31 nuclear magnetic resonance (^{31}P-NMR) of unoriented and macroscopically aligned dimyristoylphosphatidylcholine model membranes in the temperature range, 203–343 K. Lineshapes and echo intensities have been recorded as a function of interpulse delay times, temperature and macroscopic orientation of the bilayer normal with respect to the magnetic field.

The dipolar proton-phosphorus (^{1}H-^{31}P) contribution to the transverse relaxation time, T_{2E}, and to lineshapes was eliminated by means of a proton spin-lock sequence. In case of longitudinal spin relaxation, T_{1Z}, the amount of dipolar coupling was evaluated by measuring the maximum nuclear Overhauser enhancement. Hence, the results could be analyzed by considering chemical shift anisotropy as the only relaxation mechanism. The presence of various minima both in T_{1Z} and T_{2E} temperature plots as well as the angular dependence of these relaxation times allowed description of the dynamics of the phosphate head group in the ^{31}P-NMR time window, by three different motional classes, i.e., intramolecular, intermolecular and collective motions. The intramolecular motions consist of two hindered rotations and one free rotation around the bonds linking the phosphate head group to the glycerol backbone. These motions are the fastest in the hierarchy of time with correlation times varying from $<10^{-12}$ to 10^{-6} s in the temperature range investigated. The intermolecular motions are assigned to phospholipid long axis rotation and fluctuation. They have correlation times ranging from 10^{-11} s at high temperatures to 10^{-3} s at low temperatures. The slowest motion affecting the ^{31}P-NMR observables is assigned to viscoelastic modes, i.e., so called order director fluctuations and is only detected at high temperatures, above the main transition in pulse frequency dependent T_{2E}^{CP} experiments. Comprehensive analysis of the phosphate head group dynamics is achieved by a dynamic NMR model based on the stochastic Liouville equation. In addition to correlation times, this analysis provides activation energies and order parameters for the various motions, and a value for the bilayer elastic constant.

INTRODUCTION

In recent years, considerable effort has been devoted to the study of the structure and dynamics of biological membranes. Such studies are important for the understanding of the physical properties of biological membranes which control the membrane function. Among the various techniques capable of evaluating the motional characteristics of biological membranes, nuclear magnetic resonance (NMR) has played an important role (1, 2). NMR spectra provide detailed information about molecular conformation and ordering whereas relaxation time measurements probe the amplitude and time scale of the motions. Among the various nuclei present in biological membranes, phosphorus-31 (^{31}P) has particular advantages. The head group of membrane phospholipids contains an isolated $I = ½$ spin system subject only to chemical shift anisotropy and dipolar proton-phosphorus (^{1}H-^{31}P) interactions, hence, representing a well defined intrinsic probe of motion and structure (3, 4).

Address correspondence to Gerd Kothe.

Up to now, most of the ^{31}P-NMR studies on biomembranes dealt with spectra which are sensitive to restricted anisotropic motions and thus reflect the symmetry of the membrane phases. Lamellar gel-to-fluid (3), lamellar fluid-to-hexagonal (5), and lamellar fluid-to-isotropic membrane transitions (6, 7) have been detected as a function of temperature and membrane effectors like gramicidin A or melittin. So far, however, few studies have concentrated on ^{31}P-NMR relaxation time measurements. Spin-lattice relaxation studies at two different Larmor frequencies have been reported by Seelig and coworkers (8). More recently, Milburn and Jeffrey have reported similar experiments, but at four Larmor frequencies (9). In both studies chemical shift and dipole-dipole interactions have been considered in the analysis. Milburn and Jeffrey were able to show that the latter interaction dominates T_{1Z} relaxation at lower Larmor frequencies (i.e., 40 MHz) whereas the former interaction represents the major relaxation process at higher frequencies (i.e., 146 MHz). Their analysis established a unique motional process for the head group of

0006-3495/92/01/42/16 $2.00

fluid phase egg phosphatidylcholine (EPC) dispersions (9).

The aim of the present study is to describe membrane head group dynamics in a more comprehensive way. It is shown that ^{31}P-NMR can be used to probe a variety of different dynamical modes. Very fast motions are shown to affect longitudinal relaxation times at low temperatures whereas slow motions can be probed by transverse relaxation times and lineshapes at elevated temperatures. By choosing the appropriate NMR experiment, each motion can reliably be characterized. In the following we report on ^{31}P-NMR T_{1Z}, T_{2E}, T_{2E}^{CP} and lineshape measurements of dimyristoylphosphatidylcholine (DMPC) model membranes. Experiments have been carried out on both powder and macroscopically oriented samples for temperatures ranging from 203 to 343 K.

The NMR data are analyzed using a comprehensive model based on the stochastic Liouville equation. Computer simulations provide the correlation times, activation energies, and order parameters of the three different motions (intramolecular, intermolecular, and collective), necessary to account for lipid dynamics in the ^{31}P-NMR time window.

MATERIALS AND METHODS

Sample preparation

Dimyristoylphosphatidylcholine (DMPC) was purchased from Sigma Chemical Co. (St. Louis, MO) and used without further purification. Multilamellar dispersions (unoriented samples) were prepared from 300 mg of lipid with 600 mg of a 20 mM Tris buffer solution (pH = 7.4). The hydration step was performed at 313 K in a Vortex mixer. Several freeze-thaw cycles were applied to ensure sample homogeneity. The sample was then transferred into a 10-mm diameter NMR tube which was sealed under nitrogen atmosphere.

The glass slides (7 × 30 mm) employed to orient the lipid bilayers were cleaned by overnight immersion in chromic acid and then washed several times with distilled water. Oriented bilayers were prepared by coating a microscope cover slide with the multilamellar dispersion. The same procedure was applied to a second slide and subsequently repeated until a stack of ~40 slides was formed (10). The slides were then inserted into a 10-mm diameter NMR tube and sealed under nitrogen atmosphere. Finally, the sample was placed into the NMR magnet at 323 K for 2 h with the plate normal parallel to the magnetic field (annealing). The quality of orientation was continuously checked by measuring ^{31}P-NMR lineshapes. This relatively simple method provides an almost perfect macroscopic orientation of the phospholipid bilayers while keeping the sample fully hydrated.

NMR measurements

The NMR measurements were performed on a Bruker MSL-300 spectrometer operating at $\omega_o/2\pi$ = 121.5 MHz. Five types of NMR experiments were performed both on oriented and unoriented samples: (*a*) lineshape; (*b*) T_{1Z}; (*c*) nuclear Overhauser enhancement (NOE); (*d*) T_{2E} and (*e*) T_{2E}^{CP} measurements. The spin ½ Hahn-echo pulse sequence with full phase cycling of both transmitter and receiver was employed for all ^{31}P-NMR experiments (11).

^{31}P-NMR lineshapes reflecting pure chemical shift anisotropy were obtained by proton (^{1}H) spin-lock decoupling synchronized on the first radio frequency (r.f.) pulse of the echo sequence (12). The widths of the 90° pulses for ^{31}P and ^{1}H were 2.75 and 3 μs, respectively. Transverse ^{31}P spin relaxation times T_{2E} and T_{2E}^{CP} were evaluated applying Hahn-echo and Carr-Purcell-Meiboom-Gill pulse sequences, $90^\circ_x - t_1 - (180^\circ_y - 2t_1 -)_m$ (13), under ^{1}H spin-lock conditions. The spin-lock sequence was synchronized on the first pulse of the ^{31}P-NMR sequence (12). The intensity of the echo maximum as function of $2t_1$ or $2mt_1$ was fitted to an exponential law to yield the corresponding transverse relaxation time.

T_{1Z} measurements were performed by means of saturation or inversion recovery sequences, without ^{1}H decoupling. The signal recovery after saturation or inversion of the equilibrium magnetization was detected with the Hahn-echo sequence. Again, the intensity of the echo maximum as a function of the time between the saturation or inversion pulse and the first pulse of the echo sequence was fitted to an exponential law to yield the total spin-lattice relaxation rate $1/T_{1Z}$(tot) (14).

The ^{1}H-^{31}P dipolar contribution $1/T_{1Z}$(dip) to the total longitudinal relaxation rate was estimated from the maximum NOE according to $1/T_{1Z}(\text{dip}) = [2\gamma_P/\gamma_H T_{1Z}(\text{tot})][\text{NOE(max)} - 1]$ (15), where γ_P and γ_H are the respective magnetogyric ratios. Measurement of the NOE(max) was accomplished using spin-lock and Hahn-echo sequences. The spin-lock pulse was started before the application of the first 90° pulse of the echo sequence. Maximum NOE build up was estimated by following the echo intensity as a function of the delay between the start of the spin-lock pulse and the first Hahn-echo pulse. Details of the method and its applicability are given elsewhere (12).

THEORY

Spin Hamiltonian

The ^{31}P spin Hamiltonian of the phosphate head group may be written as (16):

$$\hat{\mathscr{H}}(\Omega) + \sum_{\lambda} \hat{\mathscr{H}}_{\lambda}(\Omega), \tag{1}$$

where λ stands for the magnetic interaction of interest. Here, only isotropic Zeeman ($\lambda = Z$), anisotropic chemical shift ($\lambda = CS$) and dipolar ($\lambda = D$) interactions need to be considered. Because we eliminated the dipolar contribution in all our experiments, Eq. 1 reduces to:

$$\hat{\mathscr{H}}(\Omega) = \hbar\omega_o(1 - \sigma_{iso})\hat{I}_Z - \gamma\hbar \sum_{m=-2}^{2} (-1)^m F_{2,-m}^{lab}(\Omega)\hat{T}_{2,m}, \tag{2}$$

where $\omega_o = -\gamma B_o$ is the Larmor frequency, σ_{iso} is the isotropic chemical shift and $F_{2,-m}^{lab}$ and $\hat{T}_{2,m}$ denote laboratory frame (^{lab}) spatial and spin operators of the anisotropic CS interaction, respectively. The nonzero spin operator components of this interaction tensor may be written as (16):

$$\hat{T}_{2,0} = (\tfrac{2}{3})^{1/2}\hat{I}_z B_o$$

$$\hat{T}_{2,\pm 1} = (\tfrac{1}{2})^{1/2}\hat{I}_{\pm} B_o, \tag{3}$$

where $\hat{I}_+$, $\hat{I}_-$ are the raising and lowering nuclear spin operators, respectively. The corresponding spatial elements of the CS tensor in the magnetic frame (^{mag}) can be specified as (16):

$$F_{2,0}^{mag} = (3/2)^{1/2}\delta^{CS}$$

$$F_{2,\pm 2}^{mag} = (1/2)\delta^{CS}\eta^{CS}, \quad (4)$$

where δ^{CS} and η^{CS} are the z-component of the diagonal chemical shift tensor (σ_{zz}) and the asymmetry parameter [$\eta^{CS} = (\sigma_{xx} - \sigma_{yy})/(\sigma_{zz})$], respectively. The orientation dependence of the spatial operators $F_{2,m}^{lab}(\Omega)$ in the laboratory frame can be evaluated by several coordinate transformations from the magnetic frame (X_1, Y_1, Z_1) according to:

$$F_{2,m}^{lab}(\Omega) = \sum_{m'=-2}^{2} D_{m'm}^{(2)}(\Omega)\, F_{2,m'}^{mag}. \quad (5)$$

The second rank Wigner matrix elements $D_{m'm}^{(2)}(\Omega)$ describe a series of consecutive transformations, necessary to separate the various independent motional processes. Each motion is represented by a time-dependent set of Euler transformation angles, as indicated in Fig. 1 *A*.

The intramolecular motions modulate the angles (φ_j, θ_j, ψ_j) with $2 \leqq j \leqq 4$. The intermolecular motions are represented by the time dependence of (φ_D, θ_D, ψ_D), whereas the collective motions modulate the angle (0, θ_o, 0). In addition, one has also to consider the static angular transformations (φ_1, θ_1, ψ_1), (0, θ_N, ψ_N) and (0, θ_S, 0). They describe the orientation of the magnetic tensor system in the phosphate group, the orientation of the average director relative to the sample system and the orientation of the sample system in the laboratory frame, respectively (see Fig. 1 *A*).

Density matrix

The various NMR experiments can be described by the time-dependent spin density matrix $\rho(\Omega, t)$, assumed to obey the stochastic Liouville equation (17–19):

$$\frac{\partial}{\partial t}\rho(\Omega, t) = -(i/\hbar)\mathbf{H}^{\times}(\Omega)\cdot\rho(\Omega, t) - \sum_i \Gamma_{\Omega}^{i}\cdot[\rho(\Omega, t) - \rho_{eq}(\Omega)] \quad (6)$$

Here $\mathbf{H}^{\times}(\Omega)$ denotes a superoperator associated with the spin Hamiltonian (2). Γ_{Ω}^{i} are the stochastic operators of the various motional processes, assumed to be independent, and $\rho_{eq}(\Omega)$ is the equilibrium density matrix. Introducing the reduced density matrix

$$\tilde{\sigma}(\Omega, t) = \rho(\Omega, t) - \rho_{eq}(\Omega). \quad (7)$$

Eq. (6) may be integrated to yield

$$\tilde{\sigma}(\Omega, t) = \exp\{-[(i/\hbar)\mathbf{H}^{\times}(\Omega) + \sum_i \Gamma_{\Omega}^{i}]t\}\cdot\tilde{\sigma}(\Omega, 0), \quad (8)$$

where $\tilde{\sigma}(\Omega, 0)$ denotes the initial condition of the reduced density matrix at time $t = 0$. In the presence of a strong θ_φ pulse integration of Eq. 6 leads to (20):

$$\rho(t + dt) = D^{(1)}(\varphi, \theta, -\varphi)\cdot\rho(t)\cdot D^{(1)+}(\varphi, \theta, -\varphi)$$
$$\rho(t) = \int \rho(\Omega, t)d\Omega. \quad (9)$$

Here $D^{(1)}(\varphi, \theta, -\varphi)$ is a first rank Wigner matrix and $D^{(1)+}(\varphi, \theta, -\varphi)$ is the Hermitian adjoint of $D^{(1)}$. By combining Eqs. 8 and 9, the time evolution of the spin density matrix for arbitrary pulse sequences can be calculated.

NMR observables

Generally, pulsed NMR detects the time evolution of the transverse magnetization after the n-th pulse, which can be written as

$$M(t; t_1, t_2, \ldots t_{n-1}) = \mathrm{Trace}\{\rho(t)\cdot I_+\}\exp[-i\omega(t - t_1 - t_2 \ldots - t_{n-1})], \quad (10)$$

where t_i is the separation of two consecutive pulses and ω is the angular frequency of the r.f. field. Fourier transformation of $M(t; t_1, t_2, \ldots t_{n-1})$ starting from $t = 2t_1$ (Hahn-echo sequence) yields the spectral lineshape, which may depend on the actual pulse spacing t_1. From the decay of the echo amplitude as function of t_1 (inversion recovery sequence), $2t_1$ (Hahn-echo sequence) or $2mt_1$ (Carr-Purcell-Meiboom-Gill sequence) the relaxation times T_{1Z}, T_{2E} and T_{2E}^{CP} can be evaluated. Within the Redfield limit, approximate solutions of Eq. 6, based on a time-dependent perturbation treatment, can be used (21). The appropriate expressions, relevant to this study, are developed in the Appendix.

Stochastic operators

Apparently, evaluation of the observables T_{1Z}, T_{2E}, T_{2E}^{CP} and lineshapes requires the knowledge of the stochastic operators $\hat{\Gamma}^i$ associated with the various motional processes. Intramolecular reorientations consist of motions of individual segments. In the case of the phospholipid head group, reorientation of the PO_4 tetrahedron with respect to the molecule-fixed glycerol backbone may be decomposed into rotations around the bond axes Z_2, Z_3, Z_4 (see Fig. 1 *B*). Generally, the operator for such rotations may be expressed as (16)

$$\hat{\Gamma}_j^{intra} = \frac{1}{6\tau_j}\frac{\hat{\partial}^2}{\partial\varphi_{j+1}^2}, \quad j = 1, 2, 3 \quad (11)$$

where τ_j is the correlation time for the respective motion. In the case of free rotation, $0 \leqq \varphi_{j+1} \leqq 2\pi$, whereas for restricted motion $\varphi_{j+1}^{min} \leqq \varphi_{j+1} \leqq \varphi_{j+1}^{max}$.

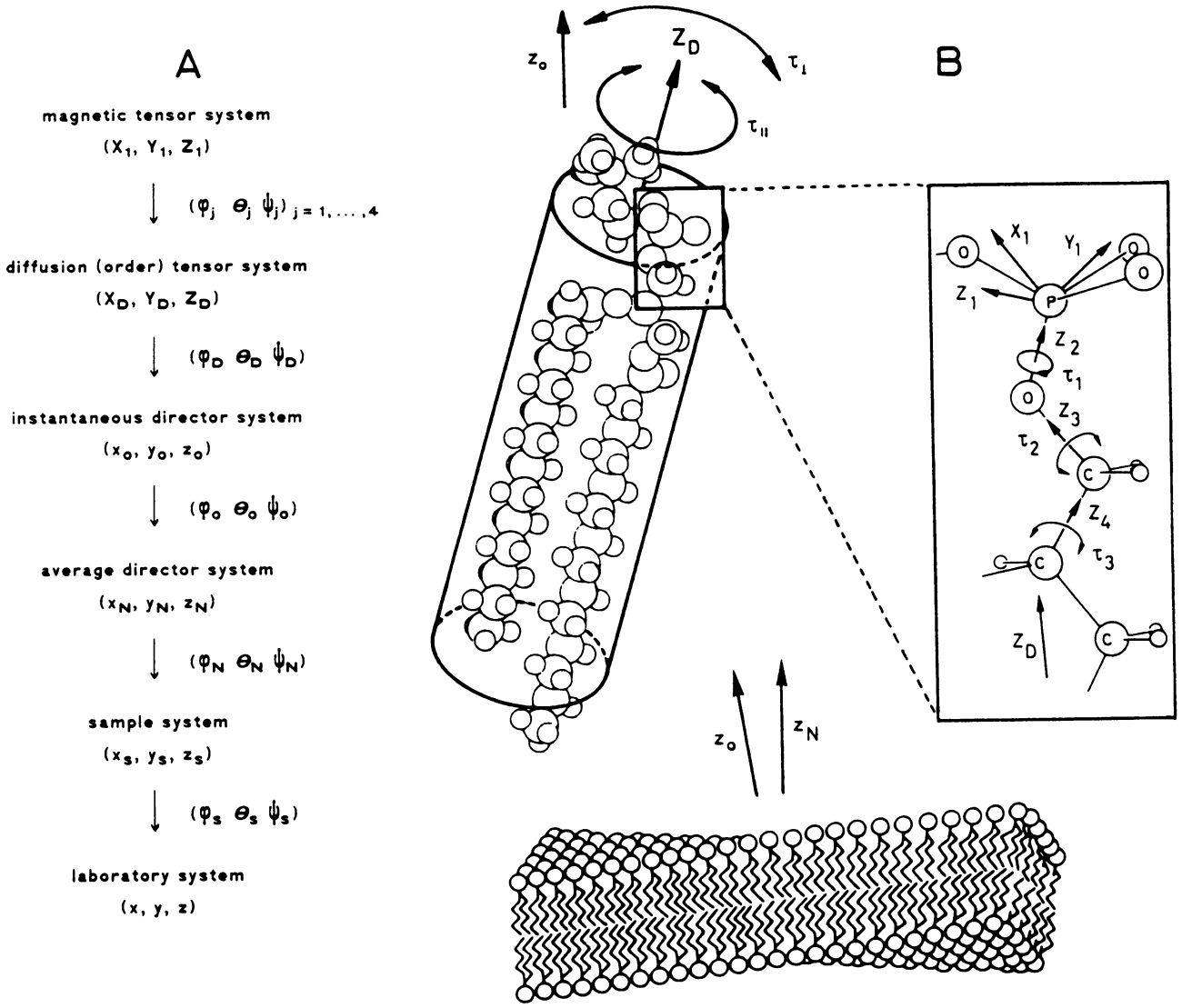

FIGURE 1 (*A*) Notation for coordinate systems and Euler transformations used in the NMR relaxation model. (*B*) Schematic representation of internal, overall, and collective lipid motions studied by ^{31}P-NMR.

Intermolecular motions are described by anisotropic rotational diffusion in an orienting potential, $U(\theta_D)$, using the operator (22):

$$\hat{\Gamma}^{\text{inter}} = \frac{1}{6\tau_\parallel}\frac{\hat{\partial}^2}{\partial\varphi_D^2} + \frac{1}{6\tau_\perp}\left[\frac{\hat{\partial}^2}{\partial\theta_D^2} + \frac{1}{k_BT}\frac{\hat{\partial}U(\theta_D)}{\partial\theta_D}\frac{\hat{\partial}}{\partial\theta_D} + \frac{1}{k_BT}\frac{\hat{\partial}^2U(\theta_D)}{\partial\theta_D^2} + \cot^2\theta_D\frac{\hat{\partial}^2}{\partial\varphi_D^2} + \frac{1}{\sin^2\theta_D}\frac{\hat{\partial}^2}{\partial\psi_D^2} - \frac{2\cot\theta_D}{\sin\theta_D}\frac{\hat{\partial}^2}{\partial\psi_D\partial\varphi_D} + \cot\theta_D\frac{\hat{\partial}}{\partial\theta_D}\right] \quad (12)$$

$\tau_\perp$ and $\tau_\parallel$ represent the correlation times for reorientation of and rotation about the long axis of the phospholipid molecule (see Fig. 1 *B*).

Collective motions are modeled as fluctuations of the instantaneous director with respect to its time-averaged orientation (see Fig. 1 *B*). For lipid bilayers two-dimensional order director fluctuations are expected (23). Within the hydrodynamic theory, these time-dependent deformations of the ordered structure are analyzed in terms of a broad distribution of thermally activated modes (24). Using a small-angle approximation, the mean square fluctuations $\langle\theta_o^2(q)\rangle$ and relaxation times $\tau(q)$ of the elastic modes can be written as (23, 24):

$$\langle\theta_o^2(q)\rangle = k_BT/(d\lambda_1^2Kq^2) \quad (13)$$

$$\tau(q) = \eta/(Kq^2). \quad (14)$$

Here, d, λ_l, K, q, and η denote a coherence length associated with the bilayer thickness, the long wavelength cutoff of the modes, the average elastic constant K of the membranes, the wave vector of mode q and the effective viscosity, respectively. The corresponding stochastic operator may then be written as

$$\hat{\Gamma}^{\text{coll}} = \sum_q \hat{\Gamma}_q[\theta_o(q)], \tag{15}$$

where $\hat{\Gamma}_q[\theta_o(q)]$ is identical with the θ_D-dependent part of Eq. 12 if $(1/6\tau_\perp)$ and $(U(\theta_D)/k_BT)$ are replaced by $[\langle\theta_o^2(q)\rangle/\tau(q)]$ and $[\theta_o^2(q)/\langle\theta_o^2(q)\rangle]$, respectively (22). Within the Redfield limit (21), a simpler approach can be used (23, 25).

To perform the numerical analysis, all differential elements of the stochastic operators are discretized according to:

$$\left[\frac{\hat{\partial}}{\partial a}p(a,\ldots)\right]_i = \frac{1}{2\Delta a}[p(a_{i+1},\ldots) - p(a_{i-1},\ldots)]$$

$$\left[\frac{\hat{\partial}^2}{\partial a^2}p(a,\ldots)\right]_i = \frac{1}{(\Delta a)^2}[p(a_{i+1},\ldots) - 2p(a_i,\ldots) + p(a_{i-1},\ldots)]. \tag{16}$$

Here a_i and Δa denote a discrete value of the general Euler angle a, and the corresponding finite differential element, respectively. The equilibrium population, $p(a_i,\ldots)$, of a particular angular position a_i is related to the normalized distribution function

$$p(a,\ldots) = \frac{1}{N}\exp\left\{\frac{-U(a,\ldots)}{k_BT}\right\} \tag{17}$$

by an integration over the area of that site

$$p(a_i,\ldots) = \int_{a_i-\Delta a/2}^{a_i+\Delta a/2} p(a,\ldots)\text{da}. \tag{18}$$

The form of the potential $U(a,\ldots)$ depends upon the model used to describe the motion. In the case of intramolecular motions we use

$$U(\varphi_j) = \begin{Bmatrix} k_BT \times N \text{ if } \varphi_j^{\min} \leqq \varphi_j \leqq \varphi_j^{\max} \\ \infty \qquad\qquad \text{otherwise} \end{Bmatrix}, \tag{19}$$

following previous studies (16). For the intermolecular motion a uniaxial potential is assumed (19, 22)

$$U(\theta_D) = k_BT \times A_{00}D_{00}^{(2)}(0, \theta_D, 0), \tag{20}$$

where the coefficient A_{00} characterizes the ordering of the molecular axes Z_D with respect to the instantaneous director z_o (see Fig. 1 *A*). Note that the conventional order parameter S_{ZZ} is related to the coefficient A_{00} by a mean-value integral:

$$S_{ZZ} = \frac{1}{2}\int (3\cos^2\theta_D - 1)p(\theta_D)\sin\theta_D d\theta_D. \tag{21}$$

A Fortran program package was employed to analyze the ^{31}P-NMR experiments. The programs calculate relaxation times and lineshapes of $I = \frac{1}{2}$ spin systems undergoing individual and collective motions in an anisotropic medium, provided CS anisotropy is the only relaxation mechanism. Numerical integrations of equation (6) are achieved employing either the Rutishauser (26) or more efficiently the Lanczos algorithm (27). Within the Redfield limit approximate solutions are employed (see Appendix).

EXPERIMENTAL RESULTS

As demonstrated in the Theory section, the different NMR observables are sensitive to motions occurring on different time scales. Generally, T_{1Z} is particularly sensitive to motions with correlation times in the range of the reciprocal Larmor frequency ω_o. Thus, by employing a high magnetic field ($\omega_o/2\pi \sim 121$ MHz) fast molecular dynamics in the range 10^{-11} s to 10^{-7} s can be studied. In contrast, T_{2E} and T_{2E}^{CP} sensitively reflect processes with correlation times equal to the inverse chemical shift anisotropy ($\Delta\sigma = (\frac{2}{3})\delta^{CS}(\omega_o/2\pi) \sim 27$ kHz), thus offering a means to study molecular dynamics in the range 10^{-7} s to 10^{-2} s. Because most motional processes are thermally activated, the variation of the sample temperature can be used to shift the correlation times into the different time windows of the NMR experiments. Therefore, ^{31}P-NMR relaxation times and lineshapes of the DMPC bilayers have been measured as a function of temperature in the range 203 K to 343 K.

Multilamellar dispersions

Fig. 2 *A* shows the temperature dependence of the spin-lattice relaxation times T_{1Z}. In the $L_{\beta'}$ phase between 203 K and 260 K, a constant decrease towards higher temperatures is observed. This behavior indicates the presence of a motion which is slow on the T_{1Z} time scale. The change in slope observed at 260 K indicates that the T_{1Z} contribution of this motion passes through a minimum. As the temperature increases above 260 K, T_{1Z} continues to decrease, showing the appearance of a second motion, which dominates T_{1Z} relaxation up to the main transition temperature, T_c (297 K). At T_c a significant drop in T_{1Z} is detected followed by a shallow

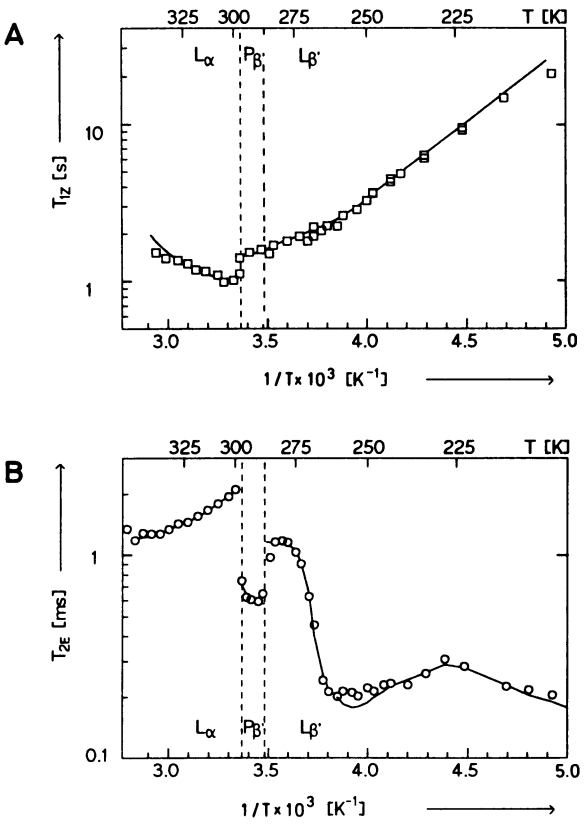

FIGURE 2 Temperature dependence of the (*A*) longitudinal (T_{1Z}) and (*B*) transverse (T_{2E}) ^{31}P spin relaxation times of DMPC in multilamellar dispersion. Dashed lines indicate different phase transitions (L_α = liquid crystalline, $P_{\beta'}$ = intermediate, $L_{\beta'}$ = gel phase). The ^{1}H-^{31}P dipolar contributions to T_{1Z} and T_{2E} were eliminated as described in the text. The solid lines represent best fit simulations of the relaxation times, employing the NMR model of the Theory section.

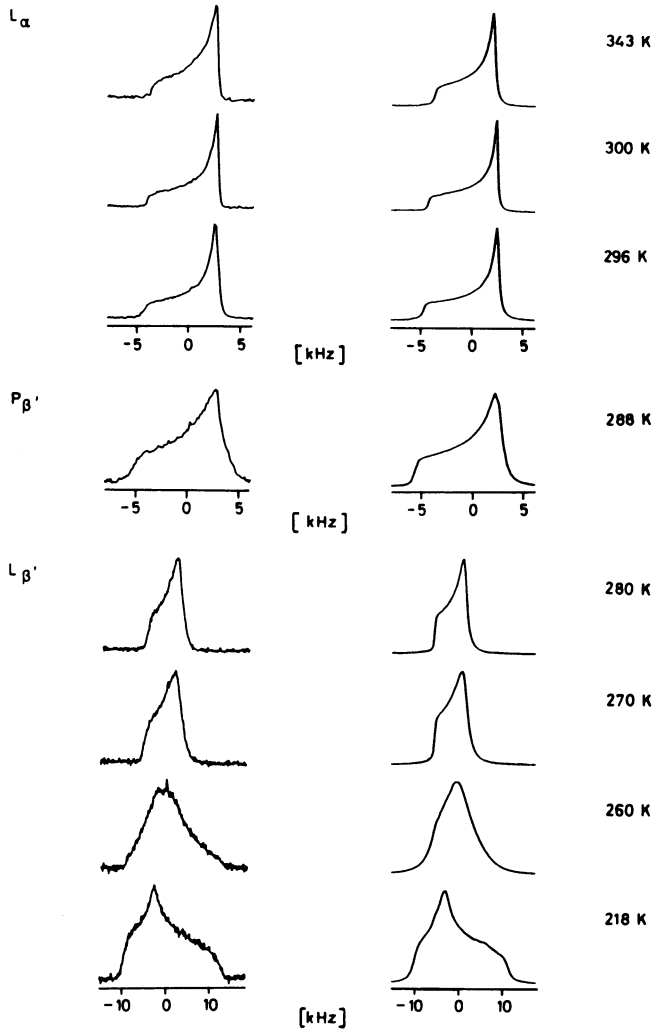

FIGURE 3 Experimental (*left column*) and calculated (*right column*) ^{31}P-NMR powder lineshapes of DMPC in multilamellar dispersion at various temperatures (L_α = liquid crystalline, $P_{\beta'}$ = intermediate, $L_{\beta'}$ = gel phase). The experimental spectra were obtained using a ^{1}H spin-lock decoupling sequence (see Materials and Methods). The simulations were performed as described in the text.

minimum and a minor increase towards the upper end of the temperature range, indicating a third motion.

In Fig. 2 *B*, the spin–spin relaxation times T_{2E} are plotted as a function of temperature. Between 203 and 230 K, T_{2E} increases, reflecting the fastest motion detectable in the T_{2E} time window. The onset of a second motion causes a decrease of T_{2E} extending up to 250 K. Then, T_{2E} passes through a minimum and increases again. The comparatively steep slope observed ~270 K indicates the presence of a third motion. The following drop at 285 K might be associated with the pretransition of the model membrane system. In the $P_{\beta'}$ phase, the increasing values of T_{2E} indicate a fourth motional process. At the main transition, T_{2E} abruptly rises by a factor of three, and then slowly levels off in the L_α phase, thus pointing to a fifth motion.

The spectral lineshapes of unoriented samples are depicted in Fig. 3. In the $L_{\beta'}$ phase, the biaxial spectral pattern detected below 250 K gradually changes to an axially symmetric lineshape with increasing temperature. The homogeneous and inhomogeneous line widths decrease up to the main transition where both drop discontinuously. Note the extended frequency scale employed for the $P_{\beta'}$ and L_α phase spectra. Above T_c, the homogeneous line width begins to increase (see Fig. 2 *B*), whereas the inhomogeneous line width continues to decrease. This can be demonstrated by evaluating the residual chemical shift anisotropy $\Delta\bar{\sigma} = (\omega_o/2\pi)[\bar{\sigma}_{zz} - (\bar{\sigma}_{xx} + \bar{\sigma}_{yy})/2]$ from the singularities of the powder spectra. The temperature dependence of $\Delta\bar{\sigma}$ is depicted

in Fig. 4. Note the discontinuities at the phase transitions and the minor overall change in the L_α phase.

Oriented samples

Generally, the use of oriented samples provides additional valuable information. Fig. 5 depicts the anisotropy of T_{1Z}, measured at various sample temperatures. The normalized values $T_{1Z}(\theta_S)/T_{1Z}$ (55°) refer to three different orientations θ_S of glass plate normal and magnetic field. In the $L_{\beta'}$ phase, the shortest spin-lattice relaxation time occurs at the "magic angle" (55°). Interestingly, this minimum gradually disappears in the $P_{\beta'}$ phase. Above T_c, a maximum of T_{1Z} at $\theta_S = 0°$ is detected followed by a steep decrease towards the 90° orientation.

Fig. 6 shows the angular dependence of the spin–spin relaxation times T_{2E}, evaluated at six different temperatures. The weak anisotropy of T_{2E}, observed at $T = 253$ K, reverses at higher temperature. For the $P_{\beta'}$ phase, an increase of T_{2E} at the 90° orientation is detected. At the main transition (297 K) the anisotropy changes significantly. Note the pronounced minimum of T_{2E} at $\theta_S \sim 45°$, measured from partially relaxed powder spectra in the L_α phase. As shown later, this angle dependence is highly indicative of the type of motion dominating transverse nuclear spin relaxation above T_c.

Fig. 7 depicts the pulse frequency ($\omega_p = 1/t_1$) dependence of the transverse relaxation time T_{2E}^{CP} obtained from Carr-Purcell-Meiboom-Gill pulse sequences. The data refer to the L_α phase at $\theta_S = 55°$ and $T = 313$ K. They have been obtained from powder samples employing a deconvolution procedure (G. Althoff and G. Kothe, manuscript in preparation). Apparently, there is a broad interval where $T_{2E}^{CP}(\omega_p)$ is proportional to ω_p^1.

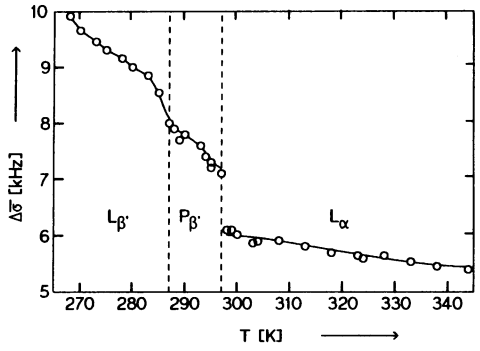

FIGURE 4 Temperature dependence of the residual ^{31}P chemical shift anisotropy $\Delta\bar{\sigma}$. The corresponding powder lineshapes were obtained using a ^1H spin-lock decoupling sequence (see Materials and Methods). The solid line represents a best fit simulation, employing the NMR relaxation model of the Theory section.

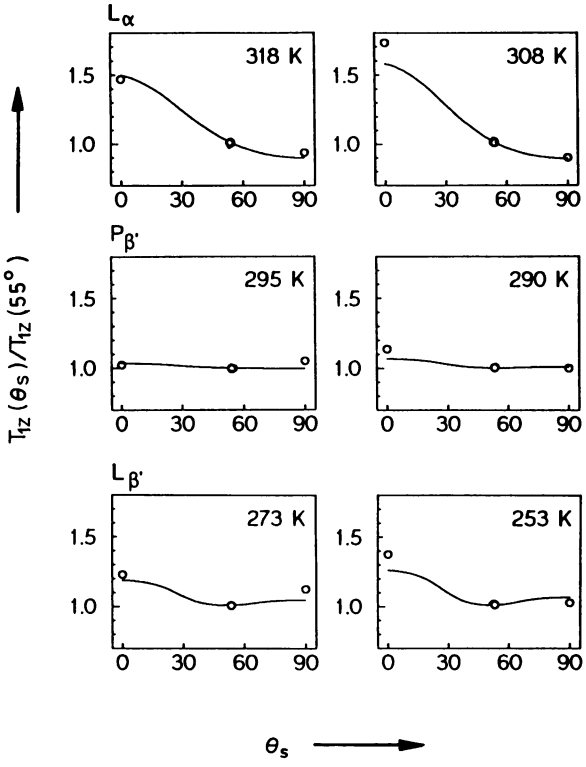

FIGURE 5 Angular dependence of the longitudinal ^{31}P spin relaxation times T_{1Z} for macroscopically oriented DMPC membranes at various temperatures (L_α = liquid crystalline phase, $P_{\beta'}$ = intermediate, $L_{\beta'}$ = gel phase). The ^1H-^{31}P dipolar contributions to T_{1Z} were evaluated by determination of the maximum nuclear Overhauser enhancement (see Materials and Methods). The solid lines represent best fit simulations of the relaxation times, employing the NMR model of the Theory section. θ_S is the angle between bilayer normal and magnetic field.

Such a linear frequency dependence is not compatible with a single motional process, characterized by a quadratic dispersion law. Rather the observed frequency dependence indicates a superposition of relaxation contributions from a large number of different modes. Prime candidates for such motions are collective order fluctuations.

Fig. 8 shows orientation dependent lineshapes of macroscopically aligned samples. Again, the scale of the frequency axis is extended for the L_α and $P_{\beta'}$ phases. At temperatures <250 K, the spectra exhibit broad biaxial shapes, reflecting slow motions and a complex orientational distribution of the CS tensor. On raising the temperature, the spectra acquire an axially symmetric shape maintained up to the main transition temperature. Above T_c fast-motional spectra with sharp resonance lines are detected for all orientations. Note, however, that the frequency positions vary drastically with the orientation angle θ_S.

DATA ANALYSIS

Combining the various experimental results, we arrive at a maximum number of eight different motions for the membrane dynamics, three being detected by T_{1Z} and five by T_{2E} measurements. However, because a particular motion can show up in the T_{1Z} and in the T_{2E} time window, the actual number of motions might reduce to five. In any case, the static spin Hamiltonian will be averaged by the various motions, according to their hierarchy in time. The strategy of the analysis follows this averaging process step by step, starting with the fastest motion in the T_{1Z} time window.

Assignment of motions

The fastest process is expected to show up at the low temperature end of the T_{1Z} plot (Fig. 2 *A*). As can be seen, T_{1Z} first decreases with increasing temperature, passing through a shallow minimum at 260 K. A value of $T_{1Z} = 2$ s at the minimum is only compatible with a highly restricted process, having a correlation time of about 1 ns ($\omega_o^{-1} \sim 1.3$ ns). Because of this short correlation time, any measurable contribution to T_{2E} can be excluded. In contrast, for the second fastest motion, no T_{1Z} minimum is detected below T_c (see Fig. 2 *A*), indicating significantly longer correlation times. Consequently, this motion might already contribute to T_{2E} relaxation at low temperatures. To reduce the number of motions to a minimum, we tentatively assign the initial slope in the T_{2E} graph to this motion (see Fig. 2 *B*). It follows that all other slower motions must show up in the T_{2E} time window, likewise.

The different slopes defining the T_{2E} minimum at 250 K (see Fig. 2 *B*) indicate the presence of two further motions. The steep increase of T_{2E} between 260 K and 280 K reveals the onset of a free rotation, as demonstrated by the change from biaxial to axially symmetric lineshapes (see Fig. 3). Hence, the two faster motions must be restricted rotations. The drop of T_{2E} at the pretransition is indicative of a fifth motion. At the main transition, drastic changes occur. The observed decrease of T_{2E} with increasing temperature, characteristic for the L_α phase, reveals a sixth motion. It turned out to be the slowest process detected by the ^{31}P-NMR experiments.

In summary, we have detected six different motional processes: two fast restricted rotations, one free rotation, one slow reorientation and two further motions of yet unknown nature. In the following, these motions are

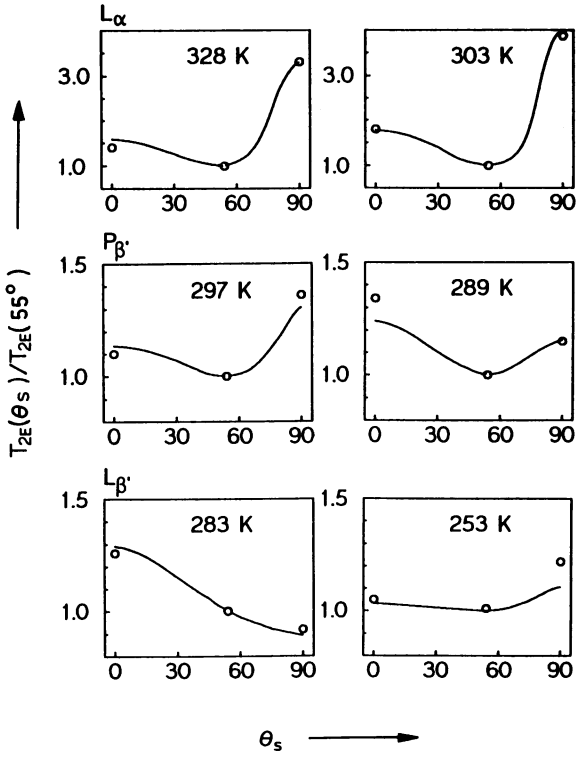

FIGURE 6 Angular dependence of the transverse ^{31}P spin relaxation times T_{2E} for macroscopically oriented DMPC membranes at various temperatures (L_α = liquid crystalline, $P_{\beta'}$ = intermediate, $L_{\beta'}$ = gel phase). The ^{1}H-^{31}P dipolar contributions to T_{2E} were eliminated by means of a ^{1}H spin-lock decoupling sequence (see Materials and Methods). The solid lines represent best fit simulations of the relaxation times, employing the NMR model of the Theory section. θ_S is the angle between bilayer normal and magnetic field.

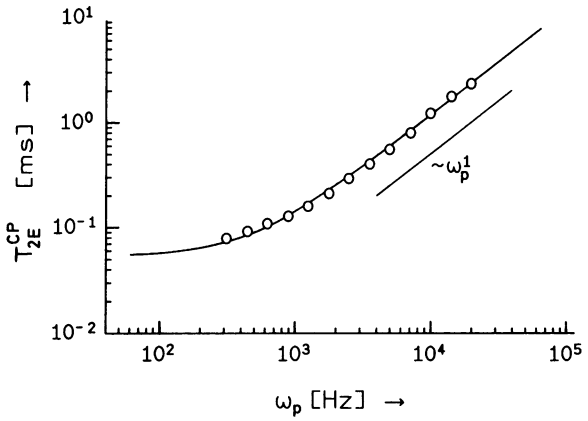

FIGURE 7 Pulse frequency ($\omega_p = 1/t_1$) dependence of the transverse ^{31}P spin relaxation times T_{2E}^{CP} obtained for DMPC membranes in Carr-Purcell-Meiboom-Gill pulse trains. The relaxation times refer to the liquid crystalline phase (T = 313 K) and θ_S = 55°. ^{1}H-^{31}P dipolar contributions to T_{2E}^{CP} were eliminated by means of a ^{1}H spin-lock decoupling sequence (see Materials and Methods). The solid line represents a best fit simulation of the relaxation times, employing the NMR model of the Theory section. θ_S is the angle between bilayer normal and magnetic field.

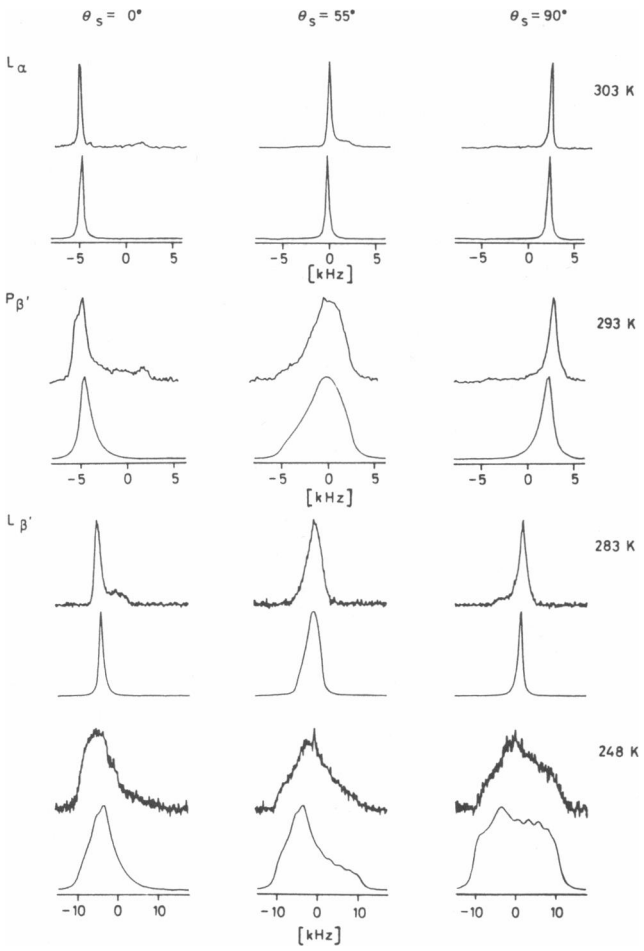

FIGURE 8 Experimental (*upper row*) and calculated (*lower row*) ^{31}P-NMR lineshapes of macroscopically oriented DMPC membranes at various temperatures (L_α = liquid crystalline, $P_{\beta'}$ = intermediate, $L_{\beta'}$ = gel phase). The experimental spectra were obtained using a ^{1}H spin-lock decoupling sequence (see Materials and Methods). The simulations were performed as described in the text. θ_S is the angle between bilayer normal and magnetic field.

assigned to particular motional processes, introduced in the Theory section. It is reasonable to classify the two fastest motions as intramolecular processes, i.e., restricted rotations about various bond axes of the phospholipid head group (librations). The problem now arises in assigning the free rotation to either an intermolecular or an intramolecular process. Deuteron (^{2}H) NMR relaxation studies of DMPC membranes, employing chain labeled phospholipids, indicate that the overall lipid rotation is frozen out at 280 K (28). Consequently, the appearance of axially symmetric ^{31}P-NMR lineshapes below this temperature results from an intramolecular process, i.e., the rotation of the phospholipid head group around the glycerol backbone. The pulse frequency dependence of T_{2E}^{CP}, observed in the L_α phase (see Fig. 7), is fully consistent with collective order fluctuations (25). Thus, the two unknown processes left are intermolecular lipid motions (29), which we describe by rotational diffusion in an orienting potential (30–32).

Characterization of motions

Once the nature and rank in the hierarchy of time is chosen for each motion, the next step is to perform the proper averaging of the CS tensor, starting from the magnetic frame of reference. The NMR observables such as T_{1Z}, T_{2E}, T_{2E}^{CP} and lineshapes are then calculated as described in the Theory section. The adjustable parameters are the correlation times and angular excursions of the motions, varied to fit the NMR observables. However, before starting the averaging procedure, the magnitude and orientation of the static ^{31}P CS tensor in the PO_4 tetrahedron must be determined.

This has been achieved by a combined analysis of orientation dependent lineshape and T_{1Z} measurements, performed at 168 K (data not shown). The results are summarized in Table 1. Angle-dependent spectra corresponding to different sample orientations at higher temperatures were submitted to an automatic least square fit analysis. The procedure, based on the efficient Marquardt algorithm (33), simultaneously calculates a series of spectra, while iteratively optimizing the model parameters employed in the fit. Thus, a reliable and consistent description of the experimental spectra can be obtained. Best fit lineshapes are shown in Fig. 3 (*right column spectra*) and Fig. 8 (*lower row spectra*). Generally,

TABLE 1 Parameters characterizing the molecular structure of dimyristoylphosphatidylcholine membranes

^{31}P chemical shift tensor elements	σ_{xx}	σ_{yy}	σ_{zz}
	ppm	ppm	ppm
Static tensor (T = 168 K)	−123	−24	147
Motionally averaged tensor (T = 248 K)	−86	−24	110
Anhydrous DPPC*	−87	−25	119
Anhydrous DMPC‡	−97	−34	133
^{31}P chemical shift tensor orientation§	φ_1	θ_1	ψ_1
Static tensor (T = 168 K)	51.6°	106°	75°
Motionally averaged tensor (T = 248 K)	55°	85°	75°
Head group geometry§	θ_2 56°	θ_3 −71.5°	θ_4 35.5°
Tilt angle of lipid molecules§	$\theta_N(L_\alpha)$ 0°	$\theta_N(P_{\beta'})$ 0° and 30°	$\theta_N(L_{\beta'})$ 30°

*Anhydrous dipalmitoylphosphatidylcholine studied by Hertzfeld et al. (34). ‡From Kohler and Klein (35). §For definition of Euler angles see Fig. 1 *A*.

the calculated spectra agree favorably with their experimental counterparts.

The result of the fitting procedure for the other NMR observables is indicated by solid lines in the Figs. 2, 4, 5, 6, and 7. Note the excellent agreement between experimental and calculated relaxation times. Optimized parameters obtained by the analysis are the Euler angles characterizing the molecular structure (see Fig. 9 *A* and Table 1), the order parameters of the lipid molecules in the various phases (see Fig. 9 *B*), the correlation times and activation energies of individual lipid motions (see Fig. 10 and Table 2) and the viscoelastic parameters characterizing collective lipid motions (Table 3).

DISCUSSION

Molecular structure

In the following, we shall first discuss the magnitude and orientation of the ^{31}P CS tensor in the polar head group (see Table 1). The evaluated tensor elements compare favorably with those of Hertzfeld et al. (34) and Kohler and Klein (35). Note that the principal values σ_{ii} reported by these authors are close to the values we found at 248 K. Apparently, these tensor elements are already averaged by internal motions. In contrast, the values obtained at T = 168 K represent the true static CS tensor. The z-component of this tensor approximately lies in the plane O_3-P-O_4 and corresponds to the highest electron density (see Fig. 9 *A*). As a consequence, the least shielded x-element is found perpendicular to this plane, approximately parallel to the O_1-O_2 vector. Our findings are in good agreement with previous results (34, 35).

Let us now discuss the head group geometry, characterized by the Euler angles θ_2, θ_3 and θ_4 (see Fig. 9 *A* and Table 1). It is noteworthy that this structural information has been obtained exclusively by NMR techniques, using macroscopically oriented samples. The values for the Euler angles closely agree with those of an x-ray study on crystalline DMPC dihydrate (36). This implies that additional hydration has apparently no effect on the head group conformation, depicted in Fig. 9 *A*. Note the preferred all-*trans* conformation of the glycerol backbone, subject to rotational isomerism about C_2-C_3 (37).

Interestingly, the geometrical parameters of the head group remain constant throughout the different phases. This result confirms previous notions, that the head group conformation is practically unaffected by the main transition (38). In contrast, the tilt angle θ_N, characterizing the orientation of the director relative to the bilayer normal, changes at the phase transitions. Note that the lipid molecules are collectively tilted by 30° in the $L_{\beta'}$ phase (see Table 1), in good agreement with results by Janiak et al. (39). No such tilt can be detected for the L_α phase. In the $P_{\beta'}$ phase the situation is more complicated as two components with different tilt angles can be distinguished in the ^{31}P-NMR experiments. Similar observations have been reported for ^{13}C-NMR studies (40). Interestingly, the obtained values of θ_N = 0° and θ_N = 30° correspond to those obtained for the L_α and $L_{\beta'}$ phase, respectively. A structural model of the $P_{\beta'}$ phase, based

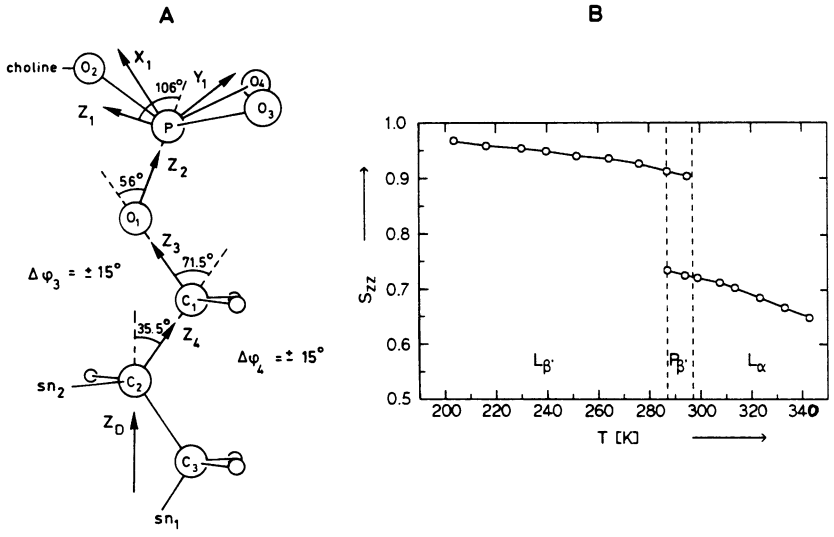

FIGURE 9 (*A*) Schematic representation of the head group geometry of DMPC membranes as determined by ^{31}P-NMR. (*B*) Temperature dependence of the orientational order parameter S_{ZZ} of the lipid molecules in DMPC membranes. Dashed lines indicate different phase transitions (L_α = liquid crystalline, $P_{\beta'}$ = intermediate, $L_{\beta'}$ = gel phase).

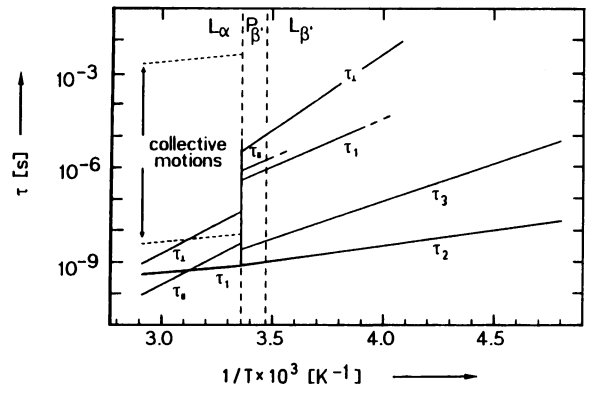

FIGURE 10 Arrhenius plot of various correlation times, characterizing internal (τ_1, τ_2, τ_3), overall ($\tau_\parallel$, $\tau_\perp$) and collective lipid motions (*marked area*) in DMPC membranes. Dashed lines indicate different phase transitions (L_α = liquid crystalline, $P_{\beta'}$ = intermediate, $L_{\beta'}$ = gel phase). τ_1 refers to head group rotation, whereas τ_2 and τ_3 characterize single-bond librations. $\tau_\parallel$ and $\tau_\perp$ are the correlation times for restricted rotational diffusion of the lipid molecules as a whole.

on a combined ^{2}H and ^{31}P-NMR study of oriented samples, will be published elsewhere (J. Stohrer, G. Gröbner, C. Mayer, E. J. Dufourc and G. Kothe, manuscript in preparation).

Molecular order

The molecular order of the DMPC membranes, as studied by ^{31}P-NMR, comprises the orientational order of the lipid molecules as a whole and the conformational order at various head group segments. Orientational order is conveniently described in terms of the familiar order parameter S_{ZZ} (see Eq. 21), characterizing the average orientation of the long lipid axes with respect to the director. In Fig. 9 *B* this order parameter is plotted

TABLE 2 Parameters characterizing individual lipid motions in the various phases of dimyristoylphosphatidylcholine membranes

Motional activation energies*		$E_a(L_\alpha)$	$E_a(P_{\beta'})$	$E_a(L_{\beta'})$
		kJ/mol	*kJ*/mol	*kJ*/mol
Head group rotation	τ_1	15	50	50
Libration around O_1-C_1	τ_2	—	20	20
Libration around C_1-C_2	τ_3	—	45	45
Overall lipid fluctuation	$\tau_\perp$	60	65	90
Overall lipid rotation	$\tau_\parallel$	60	55	—
Anisotropy ratio for rotational diffusion		$\tau_\perp/\tau_\parallel$ L_α 10	$\tau_\perp/\tau_\parallel$ $P_{\beta'}$ 10	$\tau_\perp/\tau_\parallel$ $L_{\beta'}$ —

*For assignment of motions see Figs. 1 *B* and 9 *A*.

TABLE 3 Parameters characterizing collective lipid motions in the liquid crystalline phase of dimyristoylphosphatidylcholine membranes

Viscoelastic parameters*		K	η	λ_l	λ_c
		N	cP	m	m
Data from ^{31}P-NMR‡	(T = 313 K)	1×10^{-11}	10	5×10^{-6}	—
Data from ^{2}H-NMR§	(T = 318 K)	2×10^{-11}	10	8×10^{-6}	—
Data from ^{1}H-NMR‖	(T = 303 K)	5×10^{-11}	—	—	10^{-8}

*Average elastic constant K; effective viscosity η; long wavelength cutoff λ_e of the elastic modes; short wavelength cutoff λ_c; coherence length d = 6×10^{-9} m associated with the bilayer thickness (60). ‡This work. §Stohrer et al. (25); the value of λ_l could be evaluted only by extrapolation. ‖Rommel et al. (51); the various unequivalent proton-pairs, involved in ^{1}H-NMR studies, imply a larger uncertainty in the evaluated parameters.

as a function of temperature. Dashed lines indicate different phase transitions of the DMPC membranes.

In the L_α phase, the lipid order parameter continuously increases with decreasing temperature, varying between $0.65 < S_{ZZ} < 0.72$. The values are in fair agreement with those obtained previously with ^{2}H-NMR of chain labeled lipids (28, 31, 32) and also with values obtained from electron spin resonance studies using nitroxide spinlabels (41). Apparently, the rigid body order parameter S_{ZZ} of the lipid molecules is much less than unity in the L_α phase. Thus, noncollective lipid fluctuations (see Fig. 1 *B*) are expected and there is convincing NMR evidence for their existence.

Note the weak temperature dependence of S_{ZZ} in the L_α phase. This finding is in agreement with ^{2}H-NMR results of head group labeled phospholipids (42, 43), indicating a similar small variation of the quadrupolar splitting $\Delta\nu_Q$. Because $\Delta\nu_Q$ measures the combined effect of orientational and conformational order, the temperature variation of S_{ZZ} cannot exceed 10%, as found in this study. Similar conclusions can be drawn on the basis of ^{31}P-NMR measurements of phosphatidyl-ethanolamine membranes (3).

Below the main transition the situation is more complicated. Now two lipid components with different order parameters are distinguished in our analysis. The obtained values of $S_{ZZ} \sim 0.72$ and $S_{ZZ} \sim 0.92$ correspond to those observed in the L_α and $L_{\beta'}$ phase, respectively. The fraction of the higher ordered component strongly increases with decreasing temperature. Thus, just below the pretransition, only the high order component is left. Lowering the temperature increases S_{ZZ} only slightly to a limiting value of $S_{ZZ} = 0.97$, indicating a high degree of order and tight packing of the lipid molecules in the $L_{\beta'}$ phase. Similar results have been obtained employing ^{2}H-NMR and ESR techniques (28, 31, 41).

We now discuss the conformational order at various

head group segments. As indicated in Fig. 9 *A*, there are small angle librations about O_1-C_1 and C_1-C_2 with amplitudes of $\Delta\varphi_3 = \pm 15°$ and $\Delta\varphi_4 = \pm 15°$. Using these values and $S_{ZZ} \sim 0.7$, one obtains the *C-D* bond order parameter S_{CD} for the C_1 position, in good agreement with previous measurements (43). This result indicates that the glycerol backbone actually represents the principal axis of the order and rotational diffusion tensor of the lipid molecules (see Fig. 9 *A*).

Molecular dynamics

The dynamical behavior of DMPC membranes between 203 K and 343 K, as studied by ^{31}P-NMR, is shown in Fig. 10. The graph displays logarithmic plots of the correlation times of various lipid motions as function of $1/T$. They refer to individual ($\tau_\parallel$, $\tau_\perp$) and collective reorientations of the lipid molecules and internal rotations of various head group segments (τ_1, τ_2, τ_3). The dashed lines indicate different phase transitions. We see that the Arrhenius plots are linear within a particular phase, showing discontinuities at the phase transitions. From the slopes of the straight lines, motional activation energies have been determined. They are listed in Table 2. The values of 55 kJ/mol $< E_a <$ 90 kJ/mol reflect the intermolecular character of these motions, representing reorientations of the lipid molecules as a whole. As expected, the activation energies for internal rotations (15 kJ/mol $< E_a <$ 50 kJ/mol) are smaller.

The correlation times of Fig. 10, varying by almost 10 orders of magnitude, reflect the complex molecular dynamics of DMPC membranes in the L_α, $P_{\beta'}$ and $L_{\beta'}$ phase. Note that this detailed information could be obtained only by employing various NMR relaxation techniques. For any given temperature, at least two different relaxation experiments (T_{1Z}, T_{2E}) were carried out. Moreover, evaluation of the anisotropy of the relaxation times provided additional experiments for a proper dynamic characterization of the system.

In the following, we shall discuss the various classes of motions separately, starting with the intramolecular processes. They represent small angle librations around O_1-C_1 (τ_2) and C_1-C_2 (τ_3) and a free rotation about P-O_1 (τ_1) (see Figs. 1 *B* and 9 *A*). The assignment of the latter axis is supported by previous ^{1}H-NMR studies (44). Undoubtedly, the free rotation of the phosphate group represents the most prominent motional process of the head group region (3, 35, 43, 45, 46). In the L_α phase this rotation occurs with correlation times of 4×10^{-10} s $< \tau_1 < 7 \times 10^{-10}$ s, in good agreement with recent results on dioleylphosphatidylcholine (47). At the main transition the rotational motion slows down abruptly by more than two orders of magnitude and then continues to slow more gradually upon further cooling. At $T \sim 260$ K, where water in the buffer freezes, the head group rotation is quenched. Below this temperature only small angle librations with correlation times of 10^{-8} s $< \tau_2$, $\tau_3 < 10^{-6}$ s can be detected.

It is interesting to compare the activation energies and correlation times for the intramolecular motions with those reported by Milburn and Jeffrey for EPC membranes (9). These authors observed an increase in correlation time from 10^{-9} s at 333 K to 10^{-7} s at 243 K and activation energies of 16.9 kJ/mol $>$ 265 K and 32.5 kJ/mol $<$ this temperature. Because they only studied T_{1Z} relaxation of unoriented (9) and macroscopically aligned samples (48), they could not fully characterize the motional processes. Nevertheless, their reported E_a value of 32.5 kJ/mol compares well with the average of the activation energies corresponding to the librations τ_2 and τ_3 below T_c. Moreover, their E_a value of 16.9 kJ/mol is in fair agreement with the 15 kJ/mol we report for the P-O_1 free rotation in the L_α phase. It should be noted, however, that additional motions contribute to T_{1Z} relaxation in this phase (vide infra).

As mentioned above, the intermolecular lipid motions (see Fig. 1 *B*) are modeled by rotational diffusion in an orienting potential (30–32). In the L_α phase, the correlation times for overall rotation ($\tau_\parallel$) and fluctuation ($\tau_\perp$) range from 10^{-11} s to 10^{-8} s, exhibiting a constant anisotropy ratio of $\tau_\perp/\tau_\parallel = 10$ (see Fig. 10). A motional activation energy of 60 kJ/mol reflects the intermolecular character of these motions, i.e. reorientations of the lipid molecules as a whole (see Table 2). The results are in good agreement with previous findings for DMPC membranes (28, 31, 32). Correlation times of 10^{-10} s $< \tau_\parallel, \tau_\perp < 10^{-8}$ s, expected on theoretical grounds (29), support our conclusion that restricted rotational diffusion of lipid molecules constitutes a major relaxation process in the upper megahertz regime ($\omega_o^{-1} \sim 1$ ns) (32).

At the main transition, the correlation times $\tau_\parallel$ and $\tau_\perp$ abruptly increase by more than two orders of magnitude (see Fig. 10). This abrupt slowing of the intermolecular dynamics may result from the condensing of the lipid packing when it transforms from the L_α to the $P_{\beta'}$ phase (39). Note that within the latter phase molecular rotation gradually freezes, in agreement with previous results (28). Thus, below the pretransition only slow intermolecular fluctuations are detected. An activation energy of 90 kJ/mol, evaluated for this process, reflects the crystalline character of the $L_{\beta'}$ phase.

Collective lipid motions (see Fig. 1 *B*) can only be detected by transverse ^{31}P spin relaxation in the L_α phase. The relaxation model for order director fluctuations predicts the dependence of T_{2E} on the average director orientation to be $T_{2E} \sim (\sin^2\theta_S \cos^2\theta_S)^{-1}$ (see Appendix). We find that T_{2E} is largest at the $\theta_S = 0°$ and

$\theta_S = 90°$ orientations, exhibiting the shortest value at $\theta_S \sim 45°$ (see Fig. 6). Apparently, the observed angular dependence is consistent with order director fluctuations.

Interestingly, for pulse spacings $t_1 > 1$ ms the transverse relaxation times T_{2E}^{CP} from Carr-Purcell-Meiboom-Gill sequences still exhibit a strong t_1 dependence. This result immediately shows that correlation times longer than 1 ms play an important role in the transverse nuclear spin relaxation of DMPC bilayers (25, 49). Plotting T_{2E}^{CP} as function of the pulse frequency $\omega_p = 1/t_1$ yields the relaxation dispersion curve shown in Fig. 7. Note the broad interval where $T_{2E}^{CP}(\omega_p)$ is proportional to ω_p^1. Such a linear frequency dependence is characteristic of two-dimensional order director fluctuations (23, 25), which thus constitute the dominant transverse relaxation process in the L_α phase (25, 50). Consequently, the contributions of the collective motions to longitudinal spin relaxation at $\omega_o/2\pi \sim 100$ MHz are marginal (51), in contrast to previous suggestions (52).

For pulse frequencies $\omega_p \ll (\omega_p)_1$, where $(\omega_p)_1$ denotes the low frequency cutoff of the elastic modes, the dispersion of the transverse relaxation time $T_{2E}^{CP}(\omega_p)$ should completely disappear, as observed experimentally (see Fig. 7). This finding allows an unambiguous determination of the long wavelength cutoff λ_1 of the elastic modes. In a recent ^{2}H-NMR study of DMPC membranes, λ_1 could be evaluated only by extrapolation (25). Note, however, that determination of $T_{2E} = T_{2E}^{CP}(0)$ (see Appendix) is difficult in powder samples because of the nonexponential echo decay for each director orientation (25, 53).

Analysis of the ^{31}P spin–spin relaxation measurements was performed using the relaxation model outlined in the Theory section. Optimized parameters, characterizing the hydrodynamic modes of DMPC membranes are summarized in Table 3. The bilayer elastic constant of $K = 1 \times 10^{-11}$ N and the effective viscosity of $\eta = 10$ cP compare well with those obtained previously from ^{2}H- and ^{1}H-NMR relaxation studies of the same system (25, 51). Using a completely different approach, i.e., videomicroscopy of thermally fluctuating EPC vesicles, Faucon et al. report $K \sim 1 \times 10^{-11}$ N (54), in excellent agreement with the present result. Because the elastic constant K is expected to be much larger in the crystalline $L_{\beta'}$ phase, it is plausible that collective motions are not observed in this phase.

Using the long and short wavelength cutoff of the elastic modes λ_l and λ_c (see Table 3), the dynamic range of the order director fluctuations can be estimated. As shown in Fig. 10, the collective lipid motions extend over six orders of magnitude of correlation times ranging from 10^{-9} s to 10^{-3} s. At present, one can only speculate on the biological significance of such a broad distribution of motional rates. In biological membranes the coupling of collective lipid motions to membrane-bound transporters might enhance the conformational changes necessary to the function of these proteins (50).

In a recent review on protein-lipid interactions, Bloom and Smith report that integral membrane proteins generally do not alter T_{1Z} of membrane lipids, but rather affect T_{2E} (55). In light of our findings, it thus appears that the viscoelastic properties of the membranes might be modified by the presence of proteins. Indeed, the transverse ^{2}H spin relaxation time T_{2E} of DMPC membranes was lowered by a factor of two in the presence of an integral membrane protein, indicating a corresponding decrease of the average elastic constant K (K. Weisz, N. Ryba, D. Marsh and G. Kothe, manuscript in preparation). Apparently, an enhancement of collective lipid motions is initiated upon the addition of the integral membrane protein. Thus, these proteins can communicate their presence to distant proteins via long-range protein-lipid interactions, mediated by collective lipid motions.

CONCLUSIONS

Pulsed dynamic NMR, employing naturally occurring phosphorus-31 nuclei, has been established as a powerful tool for studying biological membranes. Generally, variation of pulse sequence, pulse separation and magnetic field orientation provides a sufficient number of independent experiments necessary for a proper dynamic characterization of the systems. Analysis of these experiments in terms of molecular order and dynamics is conveniently achieved by employing a density operator treatment, based on the stochastic Liouville equation.

The studies described here provide new information concerning the dynamical organization of biological model membranes. Generally, three different motional classes can be distinguished, i.e., internal, overall, and collective lipid motions. In the gel state ($L_{\beta'}$ phase) of the bilayer membranes single-bond librations occur on the nanosecond time scale whereas head group rotation and molecular fluctuations are considerably slower, exhibiting correlation times in the micro- to millisecond range.

In the intermediate phase ($P_{\beta'}$ phase) of the lipid membranes an additional process shows up in the NMR experiments. Yet, this motion is of a molecular nature and can be interpreted as restricted rotational diffusion of the lipid molecules as a whole.

The first order gel-to-fluid phase transition promotes a considerable shift in time scale for all motions. The corresponding correlation times decrease abruptly by more than two orders of magnitude. In addition, there

appears a new class of motions in the liquid crystalline phase (L_α phase) of the membranes, i.e., order director fluctuations. These collective lipid motions are characterized by a broad distribution of thermally activated modes with relaxation times ranging from nano- to milliseconds. Analysis of the order director fluctuations provides the viscoelastic properties of the bilayer membranes.

APPENDIX

Within the Redfield limit the spin Hamiltonian (see Eq. 2),

$$\hat{H}(\Omega) = \hbar\omega_o(1 - \sigma_{iso})\hat{I}_z - \gamma\hbar \sum_{m=-2}^{2} (-1)^m F^{lab}_{2,-m}(\Omega)\hat{T}_{2,m}, \qquad (A1)$$

can be divided into a time-averaged or static part $\langle\hat{H}(\Omega)\rangle$ and a time-dependent part $\hat{H}_1(t)$. $\langle\hat{H}(\Omega)\rangle$ determines the positions of the NMR lines while fluctuations in $\hat{H}_1(t)$ give rise to spin relaxation (21). Generally, explicit expressions can be evaluated for the various relaxation times. For chemical shift anisotropy as the only relaxation mechanism, these expressions are conveniently written as

$$1/T_{1Z} = (3/4)\,(\omega_o\delta^{CS})^2 J_1(\omega_o)$$

$$1/T_{2E} = (1/8)\,(\omega_o\delta^{CS})^2[4J_o(0) + 3J_1(\omega_o)], \qquad (A2)$$

where the spectral density functions $J_m(m\omega_o)$ are the double-sided Fourier transforms of the autocorrelation function $G_m(t)$ of the fluctuating Hamiltonian $\hat{H}_1(t)$ (56).

Evaluation of $G_m(t)$ requires some model for the molecular reorientation process. As above we assume that this process can be represented by the stochastic operator

$$\hat{\Gamma}^{mol} = \hat{\Gamma}^{intra} + \hat{\Gamma}^{inter}, \qquad (A3)$$

defined in Eqs. 11 and 12. Diagonalization of Γ^{mol} yields a set of eigenvalues $\lambda^{(k)}$ and corresponding eigenvectors $X^{(k)}$, which are then used to evaluate the required autocorrelation function (32, 57):

$$G^{mol}_m(t) = (2/3)\,(\omega_o\delta^{CS})^{-2} \sum_{ij} F_{2,m}(\Omega_i)F^*_{2,m}(\Omega_j)X^{(0)}_i X^{(0)}_j \times \sum_{k\neq 0} X^{(k)}_i X^{(k)}_j \exp(-\lambda^{(k)}t), \qquad (A4)$$

where $X^{(0)}$ represents the equilibrium distribution, corresponding to the eigenvalue $\lambda^{(0)} = 0$ (see Eqs. 17–20).

The pulse frequency ($\omega_p = 1/t_1$) dependence of the transverse relaxation times T^{CP}_{2E} in Carr-Purcell-Meiboom-Gill sequences for a Markov process, characterized by a single correlation time τ_R, can be written as (13, 58):

$$1/T^{CP}_{2E}(\omega_p) = (1/2)\,(\omega_o\delta^{CS})^2 J_o(0)[1 - \tau_R\omega_p \tanh(\tau_R\omega_p)^{-1}]. \qquad (A5)$$

Here, in accordance with the high-field approximation the nonsecular spectral density function $J_1(\omega_o)$ has been neglected. On condition that $\tau_R\omega_p \geq 1$, Eq. A5 predicts a quadratic frequency dependence, $T^{CP}_{2E}(\omega_p) \sim \omega_p^2$, characteristic of a single Markov process (13, 58).

We now focus on two-dimensional order director fluctuations, analyzed in terms of a broad distribution of thermally activated modes (24). As shown previously (22, 23, 25, 59), the appropriate correlation function can be written as:

$$G^{coll}_o(t) = 3S^2 \sum_q \langle\theta^2_o(q)\rangle \exp[-t/\tau(q)], \qquad (A6)$$

where $S = \Delta\bar{\sigma}/\Delta\sigma$ is a molecular order parameter. The mean square fluctuations $\langle\theta^2_o(q)\rangle$ and relaxation times $\tau(q)$ of the elastic modes are defined in Eqs. 13 and 14. Performing the Fourier transformation and summing up the contributions of all modes between q_l and q_c, we obtain in analogy to Eq. A5:

$$1/T^{CP}_{2E}(\omega_p) = (3/2)(\omega_o\delta^{CS})^2 S^2 \sin^2\theta_N \cos^2\theta_N [k_B T/(\pi K d)] \times \int_{q_l}^{q_c} [\tau(q) - \tau^2(q)\omega_p \tanh[\tau(q)\omega_p]^{-1}]q^{-1}dq. \qquad (A7)$$

Except for $\omega_p = 0$, the integral over q has to be solved numerically. The frequency dispersion of the transverse relaxation time $T^{CP}_{2E}(\omega_p)$, predicted by Eq. A7, is not uniform over the entire range. Two different regimes can be distinguished. For a broad interval, extending from the high to the low frequency cutoff $[(\omega_p)_l < \omega_p < (\omega_p)_c]$ of the elastic modes, a linear dispersion law is predicted, $T^{CP}_{2E} \sim \omega_p^1$, characteristic of two-dimensional order director fluctuations. At lower frequencies, $\omega_p < (\omega_p)_l$, the relaxation dispersion gradually disappears and in the limit $\omega_p \to 0$ $T^{CP}_{2E}(0)$ becomes equal to T_{2E}, as indicated in Eq. A7:

$$1/T^{CP}_{2E}(0) = 1/T_{2E} = (3/2)(\omega_o\delta^{CS})^2 S^2 \sin^2\theta_N \times \cos^2\theta_N [k_B T\eta/(2\pi K^2 d)](q_l^{-2} - q_c^{-2}). \qquad (A8)$$

This research was supported in part by the Alexander von Humboldt foundation and the French-German PROCOPE exchange program. Financial support by the Deutsche Forschungsgemeinschaft and Fonds der Chemischen Industrie is also gratefully acknowledged.

Received for publication 22 May 1991 and in final form 9 August 1991.

REFERENCES

1. Davis, J. H. 1983. The description of lipid membrane conformation, order and dynamics by ^{2}H-NMR. *Biochim. Biophys. Acta.* 737:117–171.
2. Smith, I. C. P. 1985. Structure and dynamics of cell membranes as revealed by NMR techniques. *In* Structure and Properties of Cell Membranes. Vol. III. G. Benga, editor. CRC Press Inc., Boca Raton, Fl. Ch. 8.
3. Seelig, J. 1978. ^{31}P nuclear magnetic resonance and the head group structure of phospholipids in membranes. *Biochim. Biophys. Acta.* 515:105–140.
4. Smith, I. C. P., and I. Ekiel. 1984. Phosphorus-31 NMR of phospholipids in membranes. *In* Phosphorus-31 NMR, Principle and Applications. D. Gorenstein, editor. Academic Press, New York. 447–475.
5. Cullis, P. R., and B. De Kruyff. 1976. ^{31}P-NMR studies of unsonicated aqueous dispersions of neutral and acidic phospholipids. Effects of phase transitions, pH and divalent cations on the motions in the phosphate region of the polar head group. *Biochim. Biophys. Acta.* 436:523–540.
6. Dufourc, E. J., J. F. Faucon, G. Fourche, J. Dufourcq, T.

Gulik-Krzywicki, and M. LeMaire. 1986. Reversible disc-to-vesicle transition of melittin-DPPC complexes triggered by the phospholipid acyl chain melting. *FEBS (Fed. Eur. Biochem. Soc.) Lett.* 201:205–209.

7. Dufourc, E. J., J. M. Bonmatin, and J. Dufourcq. 1989. Membrane structure and dynamics by ^{2}H- and ^{31}P-NMR. Effects of amphipatic peptidic toxins on phospholipid and biological membranes. *Biochimie.* 71:117–123.
8. Seelig, J., L. Tamm, L. Hymel, and S. Fleischer. 1981. Deuterium and phosphorus nuclear magnetic resonance and fluorescence depolarization studies of functional reconstituted sarcoplasmic reticulum membrane vesicles. *Biochemistry.* 20:3922–3932.
9. Milburn, M. P., and K. R. Jeffrey. 1987. Dynamics of the phosphate group in phospholipid bilayers. *Biophys. J.* 52:791–799.
10. Hemminga, M. A., and P. R. Cullis. 1982. ^{31}P-NMR studies of oriented phospholipid multilayers. *J. Magn. Reson.* 47:307–323.
11. Rance, M., and R. A. Byrd. 1983. Obtaining high-fidelity spin 1/2-powder spectra in anisotropic media: phase cycled Hahn echo spectroscopy. *J. Magn. Reson.* 52:221–240.
12. Dufourc, E. J., C. Mayer, J. Stohrer, and G. Kothe. 1991. ^{31}P and ^{1}H NMR pulse sequences to measure lineshapes, T_{1Z} and T_{2E} relaxation times in biological membranes. *J. Chimie Physique.* In press.
13. Luz, Z., and S. Meiboom. 1963. Nuclear magnetic resonance study of the protolysis of trimethylammonium ion in aqueous solution: order of the reaction with respect to solvent. *J. Chem. Phys.* 39:366–370.
14. MacDonald, J. C. 1980. Least squares fit to some NMR functions. *J. Magn. Reson.* 38:381–384.
15. Harris, R. K. 1986. Nuclear Magnetic Resonance Spectroscopy. Pitman Books Limited, London. 250 pp.
16. Spiess, H. W. 1978. Rotation of molecules and nuclear spin relaxation. *In* NMR, Basic Principles and Progress, Vol. 15. P. Diehl, E. Fluck, and R. Kosfeld, editors. Springer-Verlag, New York. 55–214.
17. Freed, J. H., G. V. Bruno, and C. F. Polnaszek. 1971. Electron spin resonance lineshapes and saturation in the slow motional region. *J. Phys. Chem.* 75:3385–3399.
18. Norris, J. R., and S. I. Weissman. 1969. Studies of rotational diffusion through electron-electron dipolar interactions. *J. Phys. Chem.* 73:3119–3124.
19. Kothe, G. 1977. Electron spin resonance of symmetrical three spin systems in nematic liquid crystals. II. Slow-motional spectra. *Mol. Phys.* 33:147–158.
20. Schwartz, L. J., A. E. Stillman, and J. H. Freed. 1982. Analysis of electron spin echos by spectral representation of the stochastic Liouville equation. *J. Chem. Phys.* 77:5410–5425.
21. Redfield, A. G. 1965. The theory of relaxation processes. *Adv. Magn. Reson.* 1:1–32.
22. Freed, J. H. Stochastic molecular theory of spin relaxation for liquid crystals. *J. Chem. Phys.* 66:4183–4199.
23. Marqusee, J. A., M. Warner, and K. A. Dill. 1984. Frequency dependence of NMR spin relaxation in bilayer membranes. *J. Chem. Phys.* 81:6404–6405.
24. de Gennes, P. G. 1974. The Physics of Liquid Crystals. Clarendon Press, Oxford. 333 pp.
25. Stohrer, J., G. Gröbner, D. Reimer, K. Weisz, C. Mayer, and G. Kothe. 1991. Collective lipid motions in bilayer membranes studied by transverse deuteron spin relaxation. *J. Chem. Phys.* 95:672–678.
26. Gordon, R. G., and J. Messenger. 1972. Magnetic resonance line shapes of slowly tumbling molecules. *In* Electron Spin Relaxation in Liquids. L. T. Muus, and P. W. Atkins, editors. Plenum Publishing Corp., New York. 341–381.
27. Moro, G., and J. H. Freed. 1981. Calculation of the ESR spectra and related Fokker-Planck forms by the use of the Lanczos algorithm. *J. Chem. Phys.* 74:3757–3773.
28. Mayer, C., K. Müller, K. Weisz, and G. Kothe. 1988. Deuteron NMR relaxation studies of phospholipid membranes. *Liquid Crystals.* 2:797–806.
29. Pastor, R. W., R. M. Venable, M. Karplus, and A. Szabo. 1988. A simulation based model of NMR T_1 relaxation in lipid bilayer vesicles. *J. Chem. Phys.* 89:1128–1140.
30. Kar, L., E. Ney-Igner, and J. H. Freed. 1985. Electron spin resonance and electron-spin-echo study of oriented multibilayers of L_α-dipalmitoylphosphatidylcholine water systems. *Biophys. J.* 48:569–595.
31. Meier, P., E. Ohmes, and G. Kothe. 1986. Multipulse dynamic nuclear magnetic resonance of phospholipid membranes. *J. Chem. Phys.* 85:3598–3614.
32. Mayer, C., G. Gröbner, K. Müller, K. Weisz, and G. Kothe. 1990. Orientation-dependent deuteron spin-lattice relaxation times in bilayer membranes: characterization of the overall lipid motions. *Chem. Phys. Lett.* 165:155–161.
33. Marquardt, D. W. 1963. An algorithm for least-squares estimation of nonlinear parameters. *J. Soc. Indust. Appl. Math.* 11:431–441.
34. Hertzfeld, J., R. G. Griffin, and R. A. Haberkorn. 1978. Phosphorus-31 chemical shift tensors in barium diethylphosphate and urea-phosphoric acid: model compounds for phospholipid head group studies. *Biochemistry.* 17:2711–2718.
35. Kohler, S. J., and M. P. Klein. 1977. Orientation and dynamics of phospholipid head groups in bilayers of membranes determined from ^{31}P nuclear magnetic resonance chemical shielding tensors. *Biochemistry.* 16:519–526.
36. Hauser, H., I. Pascher, R. H. Pearson, and S. Sundell. 1981. Preferred conformation and molecular packing of phosphatidylethanolamine and phosphatidylcholine. *Biochim. Biophys. Acta.* 650:21–51.
37. Hauser, H., I. Pascher, and I. Sundell. 1988. Preferred conformation and dynamics of the glycerol backbone in phospholipids. An NMR and x-ray single crystal analysis. *Biochemistry.* 27:9166–9174.
38. Griffin, R. G., L. Powers, and P. S. Pershan. 1978. Head group conformation in phospholipids: a phosphorus-31 nuclear magnetic resonance study of oriented monodomain dipalmitoylphosphatidylcholine bilayers. *Biochemistry.* 17:2718–2722.
39. Janiak, M. J., D. M. Small, and G. G. Shipley. 1976. Nature of the thermal pretransition of synthetic phospholipids: dimyristoyl and dipalmitoyllecithin. *Biochemistry.* 15:4575–4580.
40. Wittebort, R. J., C. F. Schmidt, and R. G. Griffin. 1981. Solid-state carbon-13 nuclear magnetic resonance of the lecithin gel to liquid-crystalline phase transition. *Biochemistry.* 20:4223–4228.
41. Lange, A., D. Marsh, K.-H. Wassmer, P. Meier, and G. Kothe. 1985. Electron spin resonance study of phospholipid membranes employing a comprehensive line-shape model. *Biochemistry.* 24:4383–4392.
42. Gally, H. U., W. Niederberger, and J. Seelig. 1975. Conformation and motion of the choline head group in bilayers of dipalmitoyl-3-sn-phosphatidylcholine. *Biochemistry.* 14:3647–3652.
43. Seelig, J., and H. U. Gally. 1976. Investigation of phosphatidyleth-

anolamine bilayers by deuterium and phosphorus-31 nuclear magnetic resonance. *Biochemistry.* 15:5199–5204.

44. Trahms, L., and W. D. Klabe. 1985. Headgroup mobility in the low temperature phase ($L_{\sigma'}$) of DPPC. *Mol. Cryst. Liq. Cryst.* 123:333–345.
45. Kohler, S. J., and M. P. Klein. 1976. ^{31}P Nuclear magnetic resonance chemical shielding tensors of phosphorylethanolamine, lecithin, and related compounds: application to headgroup motion in model membranes. *Biochemistry.* 15:967–973.
46. Campbell, R. F., E. Meirovitch, and J. H. Freed. 1979. Slow-motional NMR line shapes for very anisotropic rotational diffusion. Phosphorus-31 NMR of phospholipids. *J. Phys. Chem.* 83:525–533.
47. Gosh, R. 1988. ^{31}P and ^{2}H NMR studies of structure and motion in bilayers of phosphatidylcholine and ethanolamine. *Biochemistry.* 27:7750–7758.
48. Milburn, M. P., and K. R. Jeffrey. 1989. Dynamics of the phosphate group in phospholipid bilayers. A ^{31}P angular dependent nuclear spin relaxation time study. *Biophys. J.* 56:543–549.
49. Bloom, M., and E. Sternin. 1987. Transverse nuclear spin relaxation in phospholipid bilayer membranes. *Biochemistry.* 26:2101–2105.
50. Watnik, P. I., P. Dea, and S. I. Chan. 1990. Characterization of the transverse relaxation rates in lipid bilayers. *Proc. Natl. Acad. Sci. USA.* 87:2082–2086.
51. Rommel, E., F. Noack, P. Meier, and G. Kothe. 1988. Proton spin relaxation dispersion studies of phospholipid membranes. *J. Phys. Chem.* 92:2981–2987.
52. Brown, M. F. 1982. Theory of spin-lattice relaxation in lipid bilayers and biological membranes. ^{2}H and ^{14}N quadrupolar relaxation. *J. Chem. Phys.* 77:1576–1599.
53. Müller, K., R. Poupko, and Z. Luz. 1990. Deuterium quadrupole and Carr-Purcell echo relaxation in chemically exchanging systems. Theory and experiments for the two-site case. *J. Magn. Reson.* 90:19–39.
54. Faucon, J. F., M. D. Mitov, P. Méléard, I. Bivas, and P. Bothorel. 1989. Bending elasticity and thermal fluctuations of lipid membranes. Theoretical and experimental requirements. *J. Phys. (France).* 50:2389–2414.
55. Bloom, M., and I. C. P. Smith. 1985. Manifestations of lipid-protein interaction in deuterium NMR. *In* Progress in Protein-Lipid Interactions. A. Watts and J. J. H. H. M. DePont, editors. Elsevier, New York. 61–88.
56. Abragam, A. 1961. Principles of Nuclear Magnetism. Oxford University Press, London. 599 pp.
57. Torchia, D. A., and A. Szabo. 1982. Spin-lattice relaxation in solids. *J. Magn. Reson.* 49:107–121.
58. Blicharski, J. S. 1986. Nuclear spin relaxation in the presence of Mansfield-Ware-4 multipulse sequence. *Can. J. Phys.* 64:733–735.
59. Vold, R. L., R. R. Vold, and M. Warner. 1988. Higher-order director fluctuations. *J. Chem. Soc. Faraday Trans.* 84:997–1013.
60. Lee, A. G. 1977. Lipid phase transitions and phase diagrams. I. Lipid phase transitions. *Biochim. Biophys. Acta.* 472:237–281.